Journal of Flow Chemistry (2020) 10:475–490
https://doi.org/10.1007/s41981-020-00105-6

REVIEW

Oscillatory flow reactors for synthetic chemistry applications

Pauline Bianchi[1] · Jason D. Williams[1,2] · C. Oliver Kappe[1,2]

Received: 2 June 2020 / Accepted: 21 June 2020 / Published online: 28 July 2020
© The Author(s) 2020

Abstract

Oscillatory flow reactors (OFRs) superimpose an oscillatory flow to the net movement through a flow reactor. OFRs have been engineered to enable improved mixing, excellent heat- and mass transfer and good plug flow character under a broad range of operating conditions. Such features render these reactors appealing, since they are suitable for reactions that require long residence times, improved mass transfer (such as in biphasic liquid-liquid systems) or to homogeneously suspend solid particles. Various OFR configurations, offering specific features, have been developed over the past two decades, with significant progress still being made. This review outlines the principles and recent advances in OFR technology and overviews the synthetic applications of OFRs for liquid-liquid and solid-liquid biphasic systems.

Keywords Oscillatory flow · Multiphasic reactions · Solid handling · Liquid-liquid reactions · Process intensification · Plug flow reactors

Introduction

Continuous flow technology has attracted the attention of chemists in recent years, specifically in scaling up hazardous chemistries, photochemistry, electrochemistry and many others [1–4]. The use of various auxiliary and automation technologies has strengthened the potential of flow reactors [5–7] for a wide range of applications [8–11]. Despite the benefits of continuous flow technology, flow reactors face some inherent problems, particularly when dealing with multiphasic systems. Rational engineering has, however, begun to tackle these issues, by developing a variety of reactor configurations with specific features aimed at processing challenging reaction media on both small and large scale [12].

One particularly promising development in reactor technology is that of oscillatory flow reactors (OFRs), whereby a symmetrical oscillation is superimposed to the net flow through the reactor. This has been found to offer a solution to multiple problems encountered by conventional flow reactors, whilst maintaining plug flow behavior, intense mixing, and excellent heat transfer. Importantly, oscillation-promoted mixing is independent of the net flow rate, opening the window of operation to lower flow rates (longer residence times), which would otherwise impart poor hydrodynamic properties. Another consequence of the ability to operate at low flow rates is the allowable decrease in reactor volume, enabling compact setups. In addition, the quality of mixing can be ensured during scale-up when OFR geometric ratios and fluidic characteristics are maintained [13].

A small number of reviews concerning OFRs do already exist, but these have focused specifically on crystallization [14], biological processes [15] or engineering developments [16, 17]. Here, we give an overview of the technological background and potential of this reactor type, aimed towards the synthetically-oriented flow chemist.

Since the efficiency of flow reactors has already been well explored for homogeneous reaction media, only a few reports examine these monophasic reactions in OFRs [18–24]. Furthermore, despite numerous studies concerning gas-liquid mass transfer in OFRs [25–27], few articles have been dedicated to synthetic applications with gases, likely due to their compressibility, which can dampen oscillations [28]. On the other hand, the high mass-transfer and continuous agitation capability of these reactors have already begun to see significant uptake for biphasic liquid-liquid and solid-liquid reactions. Consequently, this review will focus on these two classes of biphasic systems. First, the general principles and

✉ C. Oliver Kappe
oliver.kappe@uni-graz.at

[1] Institute of Chemistry, University of Graz, NAWI Graz, Heinrichstrasse 28, 8010 Graz, Austria

[2] Center for Continuous Flow Synthesis and Processing (CC FLOW), Research Center Pharmaceutical, Engineering (RCPE), Inffeldgasse 13, 8010 Graz, Austria

advantages of OFRs will be presented for each, followed by an overview of experimental reports.

Oscillatory flow reactor principles and equipment

Oscillation can be applied to a flow reactor using various oscillatory devices, such as piston- bellow-, diaphragm-, syringe- or peristaltic pumps. The symmetrical oscillation generates vortices, leading to improved radial mixing, whilst aiming to maintain plug flow character (minimal axial mixing, Fig. 1a). In this way, mixing is decoupled from the net flow and depends only on the oscillation conditions and the OFR configuration. Therefore, reactions requiring long residence times can be performed efficiently without requiring large reactor volumes. Accordingly, the numerous issues facing large volume tubular flow reactors can be obviated (e.g., high pressure drop, large footprint and poor residence time distribution).

OFRs can be characterized by different dimensionless numbers (summarized in Table 1), where the maximum oscillatory velocity is considered. Standard flow reactors require a net flow Reynolds number (Re_n) above 4000 to achieve a turbulent flow regime (Fig. 1b). However, this can be obtained at much lower Re_n in an OFR, due to the additional oscillatory turbulence, quantified by the oscillatory Reynolds number (Re_o) [14, 29]. This enables a drastic reduction of the reactor length. The plug flow behavior related to vortex cycles can be achieved at velocity ratios (ψ) between 2 and 10, depending on the baffle geometry. Usually, Re_o and St_r values larger than 100 and 0.5, respectively, are required to fully realize the benefits of OFRs.[14].

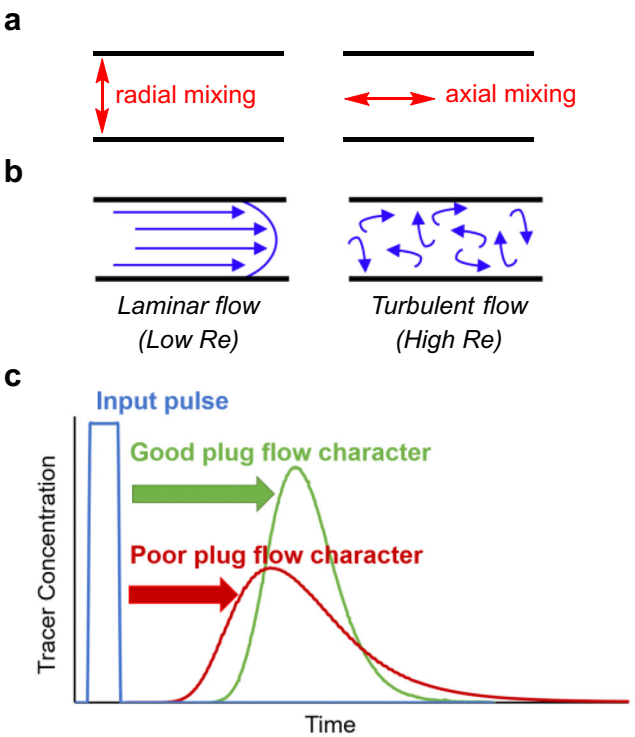

Fig. 1 Summary of mixing and flow regimes in flow reactors: **a** Radial versus axial mixing in a tube. **b** Laminar versus turbulent flow regimes. **c** Depiction of a reactor's plug flow character, estimated using tracer injection (blue) experiments, where good plug flow character has low axial dispersion (green), compared to poor plug flow character, with significant axial dispersion (red)

Residence time distribution (RTD), the distribution of time spent by the fluid within a flow reactor, is an important measure of the reactor's plug flow character. A narrow distribution decreases the probability of side reactions or incomplete reaction to occur (due to portions of material being present in the reactor for too long, or not long enough). RTD is related to the axial dispersion coefficient, which is inversely proportional to the Peclet or Bodenstein number (Table 1) [30]. RTD experiments are usually performed with a colored tracer and the dimensionless RTD parameter, E(θ), is plotted as a function of the normalized time, θ (Fig. 1c). When plug flow is achieved, a narrow symmetric curve is centered at θ = 1 (Fig. 1c, green curve). Any asymmetrical tendencies or centering at another θ suggests axial dispersion (Fig. 1c, red curve).

Axial dispersion is less sensitive to oscillatory conditions at high net flow rates, since laminar flow is minimized. Conversely, experiments with low Re_n (generally with long residence times) require careful optimization of the oscillatory amplitude and frequency to obtain a narrow RTD. Oscillation amplitude has a larger impact than frequency on the axial dispersion. At low Re_o numbers, a higher oscillation amplitude decreases the axial dispersion, thanks to the creation of vortices. After reaching a critical Re_o value, the opposite trend appears: the axial dispersion begins to increase, due to over propagation of vortices [31–34]. The optimal Re_o value depends on the net flow rate, such that the velocity ratio (ψ) still provides good plug flow character. This value must therefore be optimized for each individual reactor system.

The most common way of generating vortices is the addition of baffles within the OFR. Various baffle geometries exist and offer different degrees of mixing (Fig. 2). At each collision with an obstacle, the void behind the baffle creates a backward movement of the fluid and a short reverse flow appears. These short-lived vortices at each baffle intersection are called eddies (Fig. 3a). In continuous oscillatory baffled reactors (COBRs), oscillations lead to the generation and disappearance of eddies and therefore to homogeneous radial mixing.

The complex flow behavior in COBRs with different baffle geometries has been rigorously studied experimentally and theoretically [35–43]. However, it is still difficult to clearly quantify the impact of the geometry on reactor performance, since it depends on multiple parameters. It appears, though,

Table 1 Dimensionless numbers for characterizing oscillatory flow reactors

Dimensionless numbers	Formula [a]	Interpretation
Net flow Reynolds number	$Re_n = \frac{\upsilon \rho D}{\mu}$	Measure of the mixing intensity in net flow
Oscillatory Reynolds number	$Re_o = \frac{x_o 2\pi f \rho D}{\mu}$	Measure of the mixing intensity in oscillatory flow
Velocity ratio	$\psi = \frac{Re_o}{Re_n}$	Measure of the dominance of the oscillatory flow over the net flow
Strouhal number	$St_r = \frac{D}{4\pi x_o}$	Degree of eddy propagation in a COBR (Fig. 3a)
Dean number	$De = Re\sqrt{\frac{D}{2R_c}}$	Likelihood of Dean vortices in a coiled baffleless OFR (Fig. 3b)
Peclet or Bodenstein number	$Bo = Pe = \frac{\upsilon L}{D_a}$	Degree of axial back-mixing

[a] μ = viscosity (Pa.s), ρ = density (kg m^{-3}), υ = superficial fluid velocity (m s^{-1}), D = tube diameter (m), f = frequency of oscillation (Hz), x_0 = center-to-peak amplitude (m), R_c = radius of curvature (m), D_a = axial dispersion coefficient, L = tube length (m), h_t = heat transfer coefficient (W m^{-2} K^{-1}), k = thermal conductivity (W m^{-1} K^{-1})

that helical baffles (Fig. 2c-e) have a wide plug flow operating range, because of additional spiraling character to the net flow [36, 39, 40]. Disc and doughnut baffles (Fig. 2i) are also proposed to achieve efficient mixing at low oscillatory flow [35].

The second method for vortex generation is the use of coiled reactors instead of straight tubes [44]. A secondary flow, named Dean flow, appears due to the centripetal force arising at the curvature of the tube. The fluid near the inner wall is pushed outwards, towards the center of the tube, while an opposing current appears from the outside to the center of the coil. This superimposed flow is therefore seen as a pair of counter-rotating vortices (Fig. 3b). In coiled *baffleless* oscillatory flow coil reactors, these Dean vortices are formed and collapsed continuously during oscillations, reducing stagnation zones at their center and improving radial mixing [29]. This behavior can be quantified by the Dean number (*De*, Table 1).

A third oscillatory mixing principle is the combination with a split-and-recombine mixing structure (Fig. 3c). By applying oscillation, each of these elements will be effectively revisited numerous times by the fluid, multiplying its effect. Furthermore, these split channels have a smaller diameter, so a higher velocity (thus, higher Re_o) can be reached with a given oscillatory amplitude. This principle has received surprisingly little attention thus far, particularly considering the popularity of split-and-recombine type mixers in microfluidic applications [45, 46].

Efficient multiphasic mass transfer is another strong asset of OFRs. Studies, principally focused on gas-liquid systems in flow, have shown that the mass transfer coefficients for gas-liquid and liquid-liquid systems are generally higher than in conventional flow reactors, and remain high for a wider range of conditions, especially at low flow rates [27, 47]. Stronger oscillation (high Re_o) reduces the droplet or bubble size (until a minimal value), which increases the interfacial area. Frequency and amplitude contribute with the same weight to this enhancement [27].

Similarly, heat transfer is enhanced in OFRs compared to conventional tubes, especially at low flow rates, thanks to improved radial mixing. This enhancement depends strongly on Re_o, but not on the St_r value. The heat transfer coefficient increases with the oscillatory conditions and reaches a plateau at $Re_o \approx 1300$ [48–50]. When considering heat transfer, oscillation frequency has a higher impact than amplitude. A recent study showed that helical COBRs (Fig. 2c-e) were more efficient than central axial COBRs (Fig. 2b), followed by single orifice COBRs (Fig. 2g) in terms of thermal performance (considering both heat transfer and pressure drop) [51].

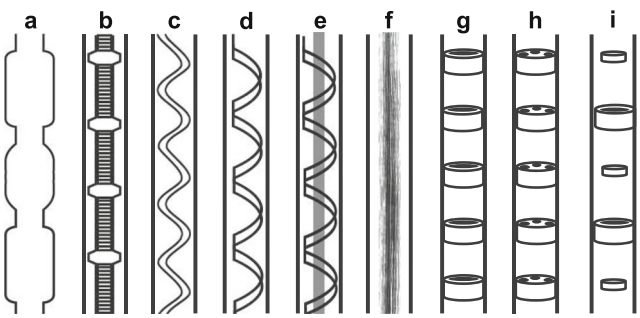

Fig. 2 Configurations of oscillatory baffled reactors. (**a**) integral baffles with periodic constrictions than can be sharp or smooth (**b**) central axial baffles (**c**) round-edged helical baffles (**d**) sharp-edged helical baffles (**e**) sharp-edged helical baffles with a central rod (**f**) wire wool baffles (**g**) single-orifice baffles (**h**) multi-orifice baffles (**i**) disc and doughnut baffles

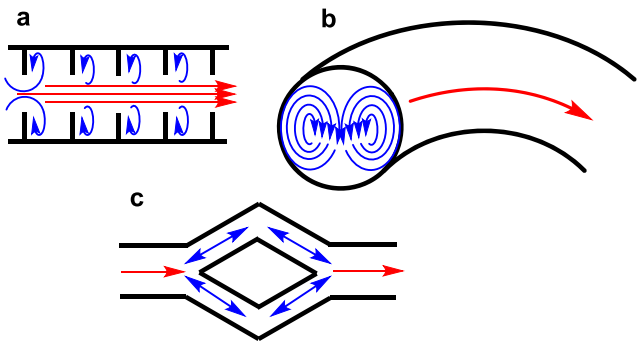

Fig. 3 Vortices generated in oscillatory flow reactors leading to improved radial mixing during oscillations. (**a**) Eddies in a continuous oscillatory baffled reactor (COBR) (**b**) Dean vortices in a baffleless OFR. (**c**) Oscillation-enhanced split-and-recombine mixing. The red arrows indicate net flow, whilst blue arrows illustrate the mixing instilled by oscillations

Another advantage of OFRs is their ease of scale-up. By keeping the dynamic parameters (Re_n, Re_o and St_r) and geometric features of the reactor (baffle spacing and open area) constant, similar axial dispersion and mixing behavior can be obtained with changing reactor volumes [13, 52]. Finally, OFRs demonstrate better performance than stirred tank reactors at similar power dissipation values. Power dissipation has been estimated using simulations based on two main models, namely the quasi-steady flow and the eddy acoustic model [53, 54].

An important factor to consider when dealing with oscillations is their dampening with distance from the oscillatory pump. The formation of air bubbles within the reactor also has a dampening effect that could be problematic for mass transfer or for the handling of solids. Pulsations are potentially unsuitable for reactions involving gases since they are compressible. Consequently, it recommended to ensure that the OFR is airtight and to consider the strength of the oscillation at the reactor outlet, prior to experimentation [52].

Nevertheless, OFRs have mostly been assessed for reactions that are inefficient in conventional flow reactors. This explains why numerous articles relying on biphasic media and solid handling have been reported. In the following sections, these applications will be discussed in detail.

Biphasic applications of oscillatory flow reactors

Liquid-liquid systems: bulk chemical applications

Experiments examining liquid-liquid systems in OFRs appeared at roughly the same time as their oscillatory batch reactor equivalent. In the late 1990s, Ni et al. studied the correlation of polymer particle size with droplet size during batch methylmethacrylate polymerization [55–58]. In the meantime, investigations into biodiesel production in OFRs took place over the course of about 15 years (Fig. 4). OFRs are good candidates for this reaction, which requires high mass transfer due to the immiscibility and difference in viscosity between triglycerides and methanol. It is only relatively recently that other biphasic chemical reactions have been reported using OFRs.

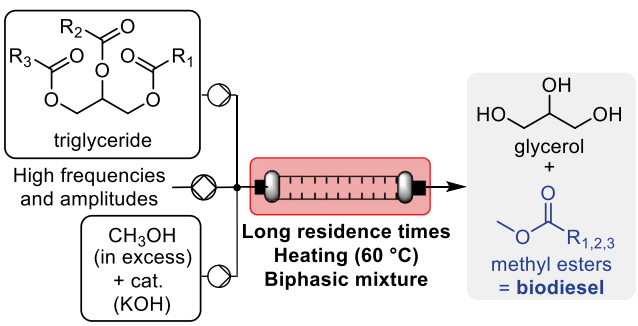

Fig. 4 General procedure for biodiesel production in a COBR

The implementation of biphasic reactions in COBRs was pioneered by the group of Harvey. In 2001, in cooperation with a sterol producer, they evaluated the batch-to-flow transition of steryl ester saponification in a meso-COBR [59]. A pair of stainless-steel pistons provided oscillations within the 1.3 L flow reactor. Thanks to a flow conversion model, based on fluid mechanics and reaction kinetics, they could lower the reaction temperature and improve the sterol yield compared to a typical batch procedure. The quality of mixing and mass transfer was high, enabling an efficient biphasic reaction between the steryl esters and ethanol. The optimal conditions found with this "tanks-in-series" modelling approach led to better selectivity for the desired sterol, despite the complex mixture at the beginning. The lab-scale tests resulted in a production of 5 kg h^{-1}, while a pilot-scale installation in the production site led to generation of sterols at about 20 kg h^{-1}.

These results were expanded upon a year later when the same group proposed a methodology for designing production-scale OFRs [13]. By using Re_o and Re_n values as the starting point for the design, different parameters could be determined, such as the power density and COBR geometry. Two experimental cases were then assessed.

The first of these cases was dedicated to the addition of an end-group, such as anhydride, to a polymer, forming a succinimide moiety [13]. The aim of this study was to obtain a productivity of 2 t h^{-1} by operating at 200 °C with a residence time of 4 h. Such a goal was seen as impractical with a simple tubular reactor because it would require a very long reactor length and high power density. These requirements were, however, achieved experimentally with a compact industrial COBR placed horizontally. The second case concerned the saponification of steryl ester [13]. Based on the previous study [59], a productivity of 50 t day^{-1} at 85 °C and with a residence of 20 min was required. A much smaller COBR configuration than in the first case was used, because this reaction involved a shorter residence time and less viscous reagents.

This reactor design methodology was also used in 2008 by Mohd et al., showing that COBRs are more powerful than standard plug flow reactors (PFRs) for biodiesel production [60]. Their simulation showed that, for a fixed reactor diameter, COBRs give higher conversion at reduced residence time than PFRs and require a lower power density.

Harvey et al. also investigated biodiesel production [61]. Their preliminary study demonstrated the potential of OFRs for this goal [62]. Then, in 2007, they showed that high oscillation frequencies were required to produce biodiesel that fulfills EU standards. Small differences between batch oscillatory baffled reactors and standard batch reactors were demonstrated. However, operating under flow conditions gave better quality biodiesel, in terms of triglyceride and diglyceride concentrations, than with a batch oscillatory baffled reactor.

In 2011, Phan et al. investigated the potential of continuous screening for biodiesel production with newly designed COBRs that allow plug flow at low Re_o [63]. Trials were first conducted at low flow rates in a meso-COBR with central sharp-edged baffles (Fig. 2b). Long experiments proved the production stability over time, with small deviations that did not depend on the oscillatory frequency. However, mixing was not sufficient and so homogeneity could not be established.

The baffles were replaced with helical round wire baffles (Fig. 2c), but insufficient mixing led to stratification of the two phases and large fluctuations in the biodiesel yield. Therefore, new baffle designs were developed to increase shear stress, resulting in the use of axially oriented sharp-edged helical baffles with or without a central rod (Fig. 2d–e). Slug flows were less prevalent with this baffle geometry, but flow channeling was still observed in the absence of the central rod. Steady-state screening was then implemented with different methanol:triglyceride ratios by using the oscillatory reactor at low Re_o. Then, dynamic screening (continuous variation of one parameter [64–66]) was assessed and results between the two screening modes were found to be in agreement.

The same year, Harvey et al. also tested three meso-COBRs with different baffle geometries for biodiesel production [67]. Depending on the configuration of the baffles, steady state was achieved after different startup times:1.5, 2.5, and 4.0 residence times for the integral, wire wool, and helical baffle designs (Fig. 2a, f, c), respectively. In each case, this startup time was shorter than that required for a single continuous stirred tank reactor. Integral baffles gave the highest content of biodiesel at high Re_o. Moreover, stable steady state was only established at high oscillatory frequencies, especially for integral baffles, otherwise mixing was insufficient to avoid stratification between the immiscible phases. The startup time decreased with increasing Re_o number - likely due to better mixing efficiency. The decrease in yield at longer residence times was related to saponification of the biodiesel. A short residence time (5–10 min) was thus required to achieve optimal biodiesel yield.

The same group has also recently published two other studies discussing homogeneous catalysis for biodiesel production from rapeseed oil: employing either 4-dodecylbenzenesulfonic acid [68], or $NaOCH_3$ [69] as the catalyst. A design of experiments (DoE) methodology was applied to determine the optimal conditions, using a meso-COBR with integral baffles (Fig. 2a).

In 2014, Mazubert et al. focused on the acid-catalyzed esterification of fatty acids from waste cooking oil into methyl esters, followed by transesterification to produce biodiesel [70]. Two fluidic reactors, namely a microstructured Corning reactor and a NiTech COBR, were compared to a batch reactor. Significant levels of conversion were achieved more rapidly for the two flow reactors than the batch one. The Corning reactor benefited from a wider operating window (higher pressure and temperature) compared to the NiTech COBR, hence speeding up the reaction further. However, reaction equilibrium was never achieved in the limited residence time allowed by this reactor. Furthermore, clogging issues occurred after long runs with high levels of free fatty acid content. On the contrary, the reaction equilibrium could be rapidly obtained even at lower temperatures in the NiTech COBR, which also showed higher flexibility in the choice of the residence time since mixing was independent from the net flow.

A comparison between two OFRs was also performed by the same group for the esterification of fatty acids from waste cooking oil. In this instance, the transesterification was done with glycerol to produce glycerides, which have applications in the cosmetics and pharmaceutical fields [71]. Contrary to the previous report [70], the two OFRs: a COBR and a baffleless OFR ("pulsed helix reactor"), were made of stainless steel to support higher temperatures and pressures. A pulsation dampener and a back pressure regulator (BPR) were employed at the reactor outlets to prevent cavitation or solvent vaporization at these elevated temperatures. Higher conversions were obtained with these reactors than with reactors operated at lower temperatures (a NiTech glass COBR and a batch reactor). The COBR showed better performance than the baffleless OFR, which the authors attributed to the generation of smaller droplets (and higher interfacial area) due to the baffles. However, higher conversion was obtained in the baffleless OFR when the acid catalyst was changed. Different experimental parameters were studied and led to higher selectivity than those previously reported in the literature.

In 2015, Lobry et al. studied liquid-liquid dispersion in a COBR for polymerization applications [72]. A first reactor configuration was developed for the liquid-liquid dispersion study. It appeared that the dispersion properties were not affected by the net flow rate, enabling dispersion-independent control of the residence time. Moreover, oscillation amplitudes and frequencies were the main parameters responsible for droplet breakage. A correlation between the droplet diameter and Re_o was determined. Conditions for obtaining stable suspensions were then successfully applied to the polymerization application.

A second reactor configuration was then designed for the polymerization of poly(vinyl acetate) (PVA) and was subdivided into different sections dedicated to: the introduction of the reagents, liquid–liquid dispersion and the reaction step. A PVA mass conversion of 30% was obtained but degassing during sampling led to encrusting on the COBR walls. The polymer particles synthesized were spherical and smooth, with a dispersion depending on the initial droplet suspension homogeneity - directly related to the oscillation conditions.

Liquid-liquid systems: fine chemical applications

Turning focus towards the synthesis of small molecules, Jensen et al. developed a multi-phase flow strategy for screening biphasic catalytic reactions on lab scale (Fig. 5) [73]. This strategy was based on a previous report by Günther et al. which demonstrated the semi-continuous preparation of gold nanorods [74, 75]. By combining oscillatory flow with an inert gas phase, this setup aimed to overcome mass transfer limitations and provide interphase mixing independent of the flow rate. The gaseous phase provided internal circulation, whilst oscillations ensured a "back and forth" movement of the aqueous slug within the organic droplet (Fig. 5a).

Three palladium-catalyzed cross-coupling reactions were assessed. First, the Suzuki–Miyaura coupling between 2-chloropyridine (**1**) and *N*-boc-2-pyrrole boronic acid (**2**) (Fig. 5c) showed that this screening setup gave similar yields to small scale batch reactors. This was in contrast to standard flow reactors, where low yields were obtained due to poor mass transfer at such low flow rates. The threshold flow rate, Q_{th}, which ensured that the aqueous segment completely passed through the organic droplet during each half oscillation, was calculated for different amplitude oscillations.

A second Suzuki–Miyaura reaction between 4-chloro-3-methylanisole (**4**) and 2,6-difluorophenyl boronic acid (**5**) emphasized the other advantage of OFRs compared to classical flow reactors: in this case, the reduction of the reactor length by a factor of 254 (Fig. 5d). The third model reaction, a Buchwald–Hartwig amination of 4-chloroanisole (**7**) with aniline (**8**) (Fig. 5e), showed the same reactivity trend across the three different reactor types, confirming the effectiveness of this strategy.

The same strategy was employed by this group for other applications which required decoupling between mixing and residence time. In the nanoparticles field, the nucleation and growth of II-VI and III-V quantum dots (QDs) were performed at various high temperatures in a similar OFR and studied by in-line absorbance measurements [76]. A biphasic ligand-exchange reaction of CdSe QDs was also performed with the single droplet OFR. The in-line UV analysis enabled determination of different exchange pathways [77]. Moreover, the strategy was easily implemented in automated platforms and integrated with purification and analysis modules, allowing high throughput screening with small volumes of various reactions for medicinal chemistry or photocatalysis applications [78–80].

In 2016, Roberge, Macchi et al. focused on the use of coiled baffleless OFRs for biphasic reactions instead of COBRs [81]. The hydrolysis of 4-nitrophenyl acetate (**10**) was used as a model reaction (Fig. 6). A BPR was put at the end of the reactor to avoid cavitation during oscillations, followed by a cyclone system for depressurization [82]. A 7-fold increase in mass transfer was calculated when Re_o was increased to 5000 by maximizing the oscillation amplitude. This improved mass transfer led to a higher conversion. A dispersed flow regime was predicted at high Re_o, with a

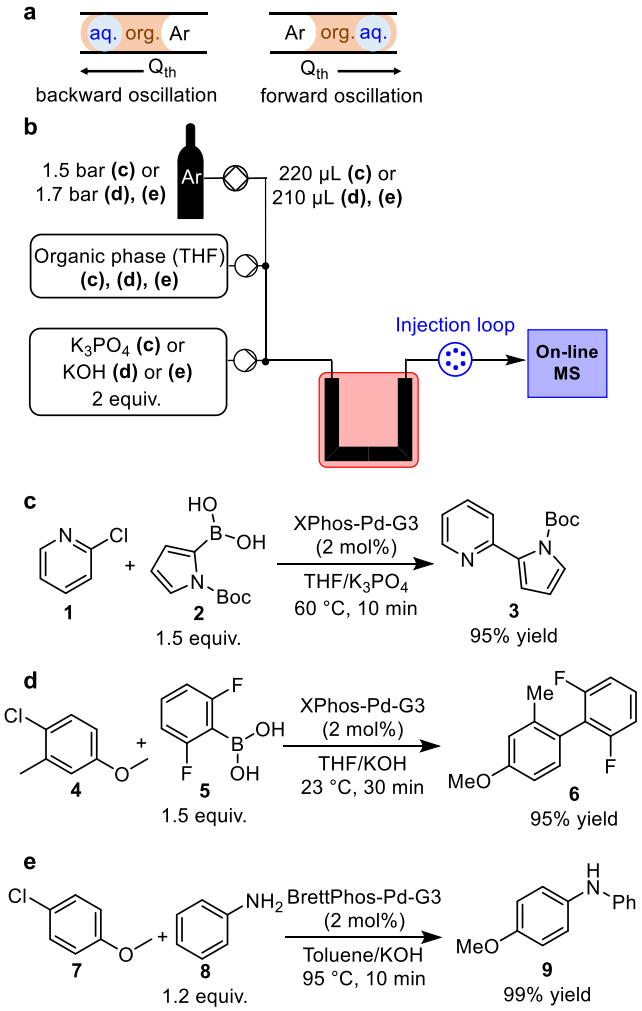

Fig. 5 Three-phase oscillatory flow strategy for small scale biphasic reaction screening. (**a**) Illustration of triphasic flow regime, showing oscillations that mix the aqueous slug back and forth within the organic slug (**b**) Schematic of the reactor setup used for this small scale screening platform (**c**) Suzuki–Miyaura coupling between *N*-boc-2-pyrrole boronic acid and 2-chloropyridine (**d**) Suzuki–Miyaura reaction between 2,6-difluorophenyl boronic acid and 4-chloro-3-methylanisole (**e**) Buchwald–Hartwig amination of 4-chloroanisole by aniline

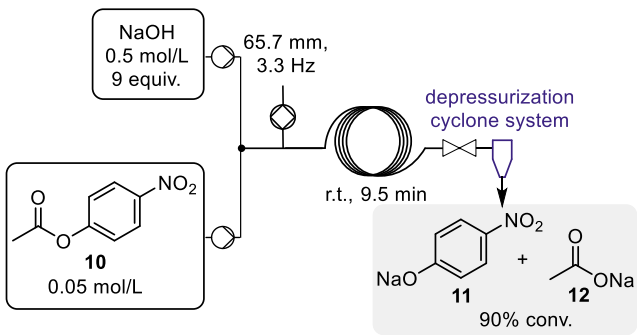

Fig. 6 Hydrolysis of 4-nitrophenyl acetate in coiled baffleless OFR

droplet diameter small enough to limit interactions with the reactor walls. In this case, oscillation frequency was found to have a more significant impact than amplitude on the mass transfer coefficient.

A comparison between these reactors and microreactor plates in terms of mass transfer performance and energy dissipation rate showed that OFRs are advantageous for slow reactions while microreactor plates are efficient for fast reactions [81]. These microreactors do appear to outperform OFRs when a sufficient droplet flow regime is not obtained in the OFR. For intermediate kinetic profiles, the authors proposed a hybrid use of both reactors because of their similar performance. These results were integrated into a microreactor toolbox for choosing the most suitable fluidic reactor by looking at the reaction rate and the phases of the medium.

In 2017, Loponov et al. developed an integrated continuous process for a biphasic reaction and in-line separation (Fig. 7). This comprised of the electrochemical generation of an oxidant, cross-flow membrane emulsification, then reaction in a COBR with smooth periodic constrictions (Fig. 2a) [83]. The dihydroxylation of styrene (**13**) by electrochemically generated ammonium peroxodisulfate [$(NH_4)_2S_2O_8$] was chosen as the model reaction. First, the use of a dispersion cell in batch proved the benefits of emulsions for overcoming mass transfer limitations and drastically reducing the reaction time.

The transposition to flow with a COBR was demonstrated and the unstable emulsion obtained at high oscillatory frequencies and amplitudes provided similar results compared to batch experiments. However, the addition of continuous membrane emulsification was needed to obtain a plug flow regime in the COBR. This setup unfortunately led to coalescence of styrene for long runs, emphasizing the need for further optimization of this method. A second COBR was placed in series and was equipped with an inlet for ethyl acetate. This strategy aimed to improve the extraction of product **14**, since it acts as a surfactant to stabilize droplets of by-products. The high oscillatory frequency and amplitude favored mixing of the two immiscible phases, hence also improving the extraction. The continuous separator module at the end of the second COBR enabled efficient extraction of **14** but also the recycling of the oxidant, improving the atom efficiency of the setup.

Over the past decade, Bjørsvik et al. have demonstrated a range of chemistries in a system termed a multi-jet oscillating disk (MJOD) reactor. This has a similar baffle structure to a COBR with multi-orifice baffles (Fig. 2h), but these baffles are attached to a central piston, which oscillates, agitating the entire length of the tubular reactor (Fig. 8a) [84, 85]. As with other OFRs, the amplitude and frequency of this oscillation can be varied, in this case with an amplitude between 0 and 25 mm and a frequency of 0–5 Hz. Amongst the chemistry examples are numerous monophasic reactions [22–24], but also several studies concerning liquid-liquid biphasic reactions.

The first of these examples was the phase transfer-catalyzed allylation of phenol **15** using allyl bromide **16** in combination with tetrabutylammonium bromide (TBAB, Fig. 8b). In this case, the batch yield of 75% in a 20 min reaction time could be matched. Interestingly, the intense mixing bestowed by this reactor also facilitated the reaction in the absence of a phase transfer catalyst. In this case, a higher reaction concentration and an extended residence time of 55 min resulted in a 60% yield [85].

A later study demonstrated the oxidation of alcohols **18** by 1,3-dichloro-5,5-dimethylhydantoin **19**, catalyzed by TEMPO (Fig. 8c). This reaction utilized a biphasic solvent system consisting of CH_3CN and a saturated $NaHCO_3$ solution, where intense mixing was provided by the oscillatory piston. Excellent yields were achieved in this transformation for a range of benzylic and other alcohols [86].

Further oxidation of the aldehyde products **20** was then achieved using more forcing conditions (Fig. 8d). The more reactive 1,3-diiodo-5,5-dimethylhydantoin **21** was required, combined with NH_4OH, longer residence time and higher temperature. A range of nitriles **22** were obtained in good to excellent yields using this protocol in flow. This second oxidative transformation involves the attack of NH_4OH on the carbonyl and, under certain conditions (high NH_4OH concentration), alternative diaziridine or hydrazine derived products could be obtained, but with relatively low selectivity [86].

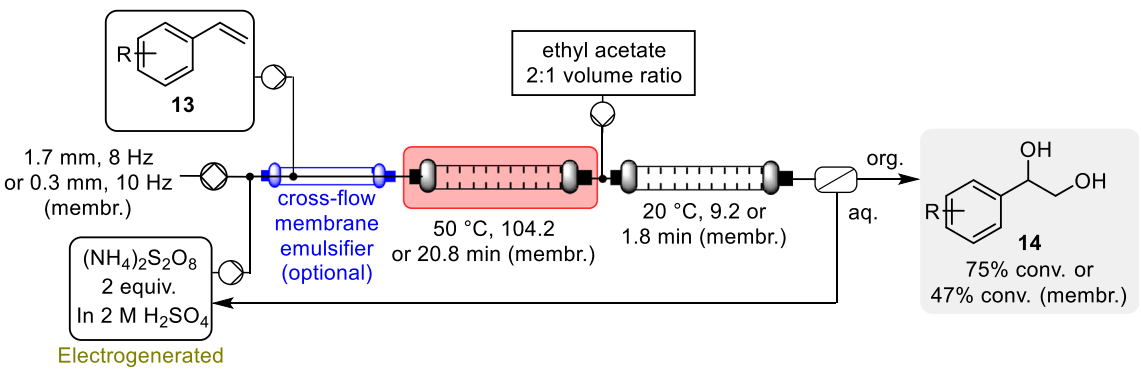

Fig. 7 Three-stage emulsification, oxidation and separation, allowing oxidation of styrene using an electrochemically generated and recyclable oxidant in a COBR

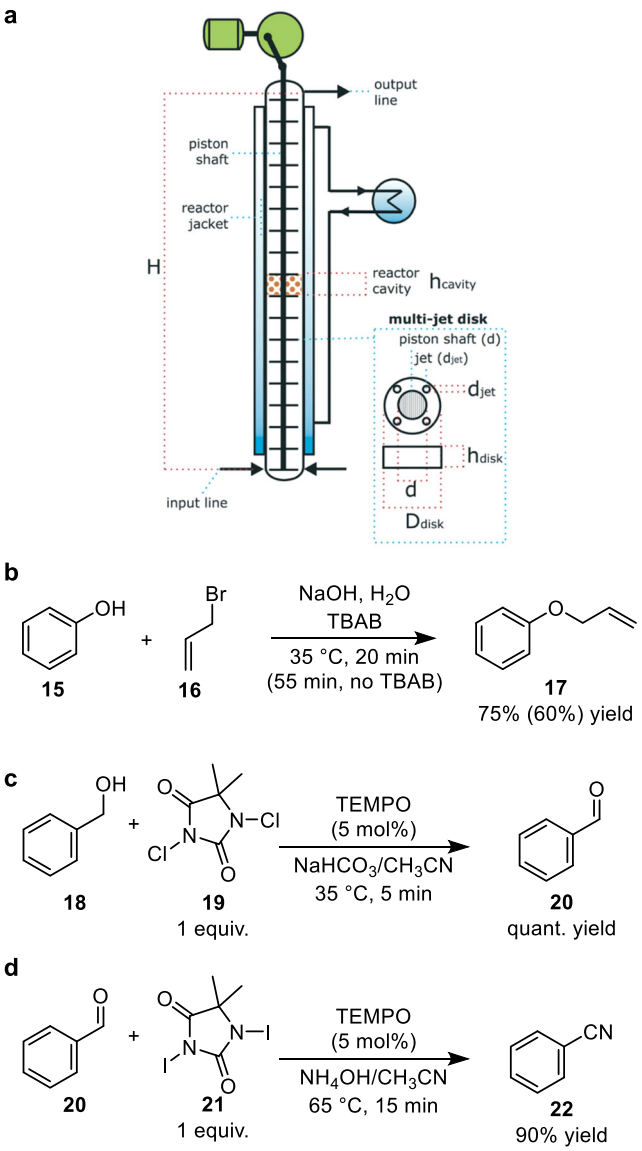

Fig. 8 Biphasic applications of a MJOD reactor. (**a**) Schematic diagram of the MJOD reactor including details of disk structure. (Reprinted with permission from Ref [85]. Copyright (2019) Royal Society of Chemistry) (**b**) Phase transfer catalyzed allylation of phenol (**c**) Oxidation of alcohols to their corresponding aldehydes (**d**) Further oxidation of aldehyde products in the presence of NH_4OH to yield nitriles

Solid-liquid systems: general principles

The use of solids in organic chemistry is very attractive, since their separation from the reaction medium is easy to achieve, reducing the cost and time needed for downstream purification. Solids can be either a catalyst, reagent or product, which explains their occurrence in many processes for active pharmaceutical ingredient (API) production, biomass valorization and other applications. Despite the advantages of continuous flow technology, handling solids remains very challenging due to the use of narrow reactor channels, which are susceptible to clogging [87]. Without high flow velocities, solids can also settle in a flow reactor, depending on the properties of the reactor, the solid and the reaction medium. Moreover, feeding solids from pumps is another difficult task. Working at temperatures higher than the melting point of the solid can occasionally provide a solution, but is by no means a universal approach and requires an intensive optimization process [88, 89].

To overcome such issues, various continuous flow strategies have been adopted [90]. Packed-bed reactors are often viewed as a good solution for heterogeneous catalysis, but they suffer from uncontrolled fluid dynamics (including channeling), heat transfer limitations and high pressure drop (which complicates scale-up) [91–94]. Other approaches use active mixing to suspend solids without fouling. Continuous stirred tank reactors [95–97] and agitated cells [98, 99] have been shown to achieve such mixing, as well as the use of sonication [100, 101]. However, these reactors possess a poor RTD, especially when the vessel size is large. The addition of a screw within the fluidic reactor has also recently received attention but this setup does not support gas formation or liquid settling and is only suitable for fast reactions [102–105]. Finally, suppression of fouling can often be achieved by generating a slug flow regime, using an immiscible carrier phase which has minimal interactions with the reactor walls. Scaling up such processes is challenging, though, since larger tube diameters limit the formation of these Taylor flow regimes [106, 107].

In this context, OFRs have emerged as an effective tool for handling solids. Oscillations afford enhanced mixing, which can prevent clogging and solid deposition or sedimentation on the reactor walls. Besides, the configuration of such reactors enables facile scale-up and meso-OFRs have already seen use for solid-liquid reactions. Finally, in contrast to other fluidic reactors, it is possible to improve the efficiency of the reaction within OFRs by simply optimizing the frequency and amplitude of the oscillation.

Frequency and amplitude of the oscillation have been demonstrated to have a significant effect on solid suspension. Nikačević et al. have distinguished different flow patterns in a COBR, depending on the oscillatory velocity and, therefore, the power input of the COBR [108]. The oscillatory velocity must be high enough to overcome sedimentation, otherwise, particles move very slowly at the lowest part of the reactor (Fig. 9a). Solid suspension can then be either non-uniform (Fig. 9b) when the settling still occurs, or uniform (Fig. 9c) at high oscillatory velocity.

Recent studies on the axial dispersion of solids in OFRs have demonstrated that solids and liquids do not experience the same degree of axial dispersion, so the oscillation parameters must be tuned accordingly.

In 2017, Reis et al. determined the most favorable geometrical parameters of a COBR for homogeneously suspending solid particles and minimizing the solid axial

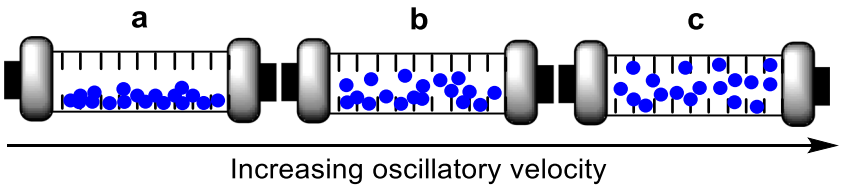

Fig. 9 Effect of the oscillatory velocity on the solid flow regimes in an oscillatory flow reactor (**a**) settling of solids (**b**) non-uniform suspension of solids (**c**) uniform suspension of solids

dispersion [109]. Optical imaging of suspended polyvinyl chloride (PVC) particles was implemented to determine the RTD of various COBRs using a DoE approach. The results showed that solids experience a longer residence time than liquids due to the strong vortices generated. Moreover, COBRs with integral *smooth* periodic constriction baffles (Fig. 2a) require lower oscillation amplitudes to fully suspend solid particles than COBRs with the equivalent *sharp edged* periodic constriction baffles. Finally, the cross-sectional area of the tube was found to be the most dominant parameter for controlling back mixing of the solid particles.

The same year, Kramer et al. studied the effects of oscillation frequency and amplitude on the axial dispersion of liquids and solids in a COBR [110]. Methylene blue was the liquid tracer and was followed by absorbance measurements, while melamine (the solid tracer) was monitored using focused beam reflectance measurements. The results indicated that the minimum axial dispersion for solids was obtained at low oscillation amplitudes, but the frequency has less impact on this parameter. This study also suggested that velocity ratio, ψ, alone is not enough to identify optimal operating conditions. The same conclusions were reached two years later by Cruz et al. for planar oscillatory flow crystallizers [111]. Nagy et al. also confirmed these observations and found that oscillatory pumps afford a larger solid dispersion due to back mixing, compared with net flow pumps. However, this does not detract from their essential character for preventing particles from settling and clogging [112].

More recently, Rielly et al. used a dual backlit imaging technique to simultaneously assess the RTD of the liquid and solid phases in a meso-COBR with integral smooth periodic constriction baffles (Fig. 2a) [113]. This non-invasive technique was not subjected to errors that could result from using two different measurement techniques for the tracers (Procion Red HE-7B dye and polystyrene particles). A range of Re_0 values was measured for solid-liquid plug flow and it was shown that the difference in axial dispersion experienced by solids and liquids is less pronounced at higher oscillation frequency.

From all of these studies, it appears that a compromise between efficient particle suspension and narrow RTD (minimal axial dispersion) has to be found during the optimization of heterogeneous reactions in OFRs.

Solid-liquid systems: synthetic applications

Studies of solid-liquid chemical reactions in oscillatory *batch* reactors first appeared around 20 years ago, where stable suspensions of TiO_2 particles were achieved for the photochemical oxidation of methylene blue and salicylic acid [114–116]. The first use of OFRs for solid-liquid systems appeared a decade later and was focused on the use of COBRs packed with a heterogeneous catalyst. More recently, the suspension of solid particles in a slurry flow has also been demonstrated in OFRs.

In 2013, Harvey et al. proposed a protocol for the heterogenous acid-catalyzed esterification of carboxylic acids with methanol in a meso-COBR [117]. The catalyst consisted of a suspension of SBA-15 silica derivatized with propylsulfonic acid ($PrSO_3H$-SBA-15). Its turnover frequency (TOF) was demonstrated to be higher in continuous flow than stirred batch conditions. Water poisoning was responsible for the catalyst deactivation, but this phenomenon was less pronounced in flow, thanks to the plug flow formed in the meso-COBR, which was proposed to decrease the number of water molecules accessing the resin surface. It was also proven that oscillations were required to avoid sedimentation of the particles, but the reaction was mixing independent.

The same group published another study relating to the use of a more efficient catalyst (Fig. 10) [118]. This time, the reactor was packed with the Amberlyst 70-SO_3H resin, which is composed of a copolymer of divinylbenzene and styrene, functionalized with sulfonic acid. The TOF calculated for this catalyst was higher than that previously reported for $PrSO_3H$-SBA-15. Water deactivation was not observed with the new catalyst, which showed good stability over time. The recovery of the resin after water-spiking was facilitated by the water-resistance of Amberlyst 70-SO_3H and the continuous flow of reagents.

Three screening modes were tested in order to find the optimal reaction parameters for the reaction between hexanoic acid (**23**) and methanol. These were: multi-steady states (waiting for steady state to be reached between varying each parameter), dynamic (continuous variation of one parameter) and multi-dimensional (dynamically varying two parameters at the same time). With the first mode, the highest yield (95.4%) of methyl hexanoate (**24**) was obtained at 20 min residence time with a methanol:carboxylic acid ratio of 30:1. Similar results were achieved between the multi-steady state

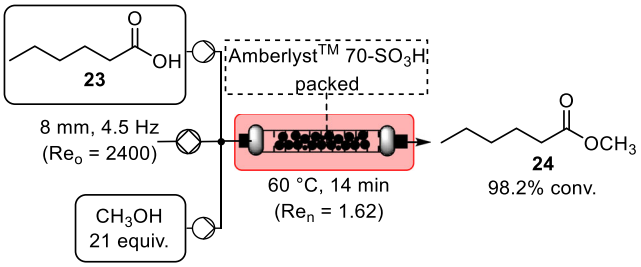

Fig. 10 Heterogenous acid-catalyzed esterification of hexanoic acid with methanol with a meso-COBR

and the dynamic modes, but the dynamic mode decreased the required screening time by about 16%. Finally, in the multi-dimensional mode, the highest yield of **16** (98.2%) was achieved with a shorter residence time of 14 min and lower methanol:carboxylic acid ratio of 21:1.

One year later, Harvey et al. proposed another protocol which combines biodiesel production from triglycerides with the valorization of the glycerol by-product [119]. This study employed a meso-COBR packed with different Amberlyst resin catalysts, in a process which could be carried out in one or two stages (Fig. 11). The transesterification of triacetin (**25**) was assessed with two resins: the first was basic (Amberlyst A26-OH) and the second acidic (Amberlyst 70-SO_3H). The basic catalyst led to a higher reaction rate and TOF than the acidic one. However, this basic catalyst was water-intolerant and was irreversibly deactivated, even in the continuous flow of fresh reagents.

Then, the reaction between glycerol and acetone (**26**) was studied in the presence of methanol. The single-stage process consisted of a stream containing methanol, triacetin and acetone in a 30:1:4 ratio. The catalyst used was the acidic Amberlyst 70-SO_3H resin. After 30 min residence time, only 48.5% of solketal

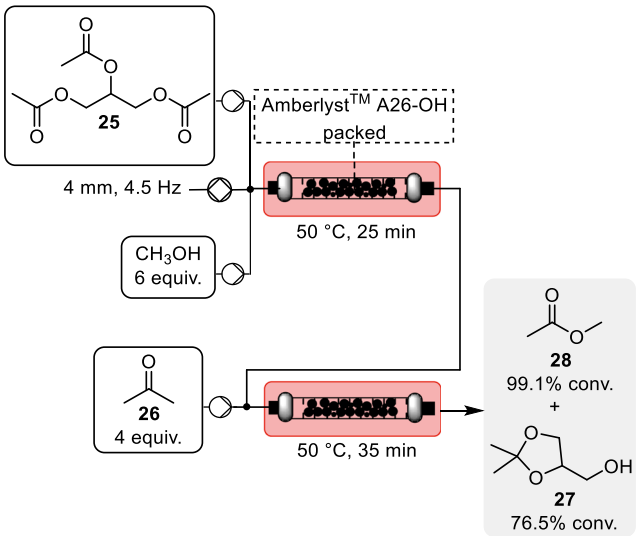

Fig. 11 Concomitant formation of the biodiesel methyl acetate and solketal from glycerol valorization in a packed meso-COBR during a two-stage process

(**27**) and 95.3% of methyl acetate (**28**) were obtained at 50 °C, proving the two-stage process to be more efficient. The first reactor for the esterification was packed with the basic Amberlyst A26-OH resin and connected to the second one, containing the acidic Amberlyst 70-SO_3H resin for the acetylation. Better yields of **28** (99.1% in 25 min residence time) and **27** (76.5% in 35 min residence time) were obtained, because less methanol was required for this process (6 equivalents instead of 30) and the first reaction was more efficient with the basic resin. Finally, around 76% of glycerol content was valorized into **27**, considered as an additive to the biodiesel fuel produced during the transesterification step.

In a related transformation, Yunus et al. performed the semi-quantitative conversion of palm fatty acid distillate (PFAD) into biodiesel with a new glucose acid catalyst [120]. This catalyst was characterized by various techniques before being used as a suspension in the meso-COBR. Different parameters, such as catalyst loading, temperature, oscillation frequency, residence time and methanol:PFAD ratio were optimized. The produced biodiesel showed similar properties to petroleum and diesel fuel standards.

In 2017, a miniaturized COBR was manufactured by stereolithography-based 3D printing for the preparation of stable silver nanoparticles (Ag NPs) (Fig. 12) [121]. This cheap, high-quality and fast manufacturing enabled the construction of a small scale COBR resistant to high pressures and inert to various solvents. For the sake of offering a cheap and easy setup, a syringe pump was used to generate oscillation. This was equipped with a syringe filled with an immiscible silicon oil to prevent back mixing of the reagents. By estimating the dimensionless RTD E(θ), thanks to absorbance measurements with a methylene blue tracer, the RTD within the mini COBR was proven to be narrower than in a similar tubular reactor. The experimental results of E(θ) fit well with an axial dispersion model.

The mixing quality was improved by increasing the frequency and the amplitude of the oscillation since it led to a higher Peclet number. The velocity ratio, ψ, was high due to the relatively low net flow rate. The mixing efficiency was advantageously exploited for the continuous flow synthesis of Ag NPs. $AgNO_3$ in acetonitrile was used as the silver

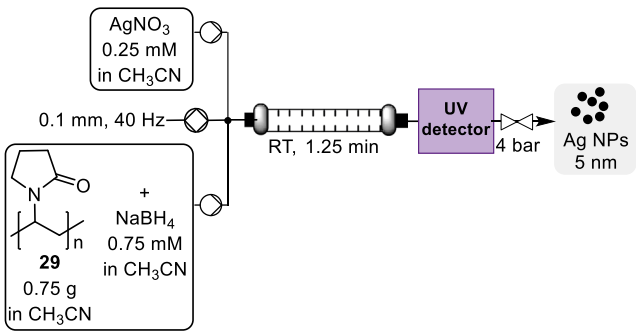

Fig. 12 Synthesis of silver nanoparticles in a miniaturized COBR

source, $NaBH_4$ as the reductant and polyvinylpyrrolidone (**29**) as the stabilizer. TEM and in-line UV-VIS analyses showed that Ag NPs produced in the mini COBR were more uniform and stable than those synthesized with a standard tubular reactor. Reactor fouling was also less pronounced with the mini COBR. A low oscillation amplitude and frequency were, however, required to ensure NP monodispersity.

In 2018, Zheng et al. used an oscillatory generator and a meso-COBR packed with an acid-cation exchange resin (NKC-9) as a heterogeneous catalyst for the acetylation of camphene **30** (Fig. 13) [122].

The residence time distribution of this reactor was proven to be close to that of an ideal PFR. The time needed to reach equilibrium was shorter under flow than batch conditions because of improved heat- and mass transfer. A similar trend was observed for the yield and selectivity for isobornyl acetate (**32**). The specific surface area and pore volume of the catalyst after 30 h of processing in a COBR were similar to those of the fresh catalyst. Moreover, the catalyst particles were less prone to the formation of a by-product layer at their surface in a COBR than in a round-bottom flask, although high oscillatory amplitudes could induce the formation of cracks.

Bjørsvik et al. have also been studied various solid-liquid reactions in the previously introduced MJOD reactor (Fig. 8a). These include reactions where solids are fed into the reactor as a slurry, but also cases with solid reaction products being formed in the reactor itself. One of the studies discussed in the initial report of this reactor demonstrated a Hofmann rearrangement, where the benzamide substrate **33** was fed as a slurry in 1,4-dioxane (Fig. 14a) [85]. The desired aniline product **34** could be isolated in quantitative yield after 15 min residence time at 80 °C.

A reagent which has been the focus of two studies from the same group is 1,3-diiodo-5,5-dimethylhydantoin **21**, whose preparation and onward reaction have both been studied using this reactor. The preparation of **21** was achieved by reacting 5,5-dimethylhydantoin **35** with ICl in a basic biphasic medium (Fig. 14b). In this case, the optimal oscillation frequency

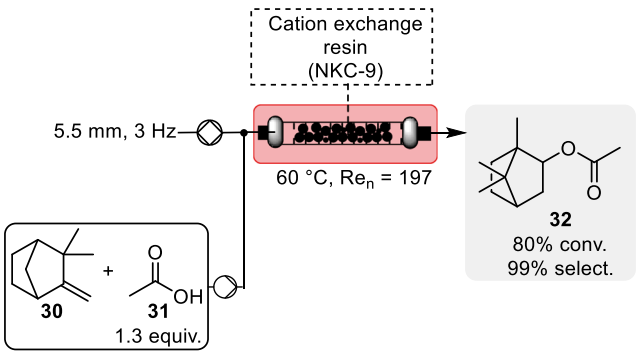

Fig. 13 Heterogenous acid-catalyzed acetylation of camphene in a meso-COBR

was found to be 1.6 Hz, since higher frequency was proposed to produce smaller product particles, which could not be effectively recovered by filtration at the reactor outlet [123]. A separate study on the use of this iodinating agent **21** was originally attempted using a slurry feed, but clogging problems were observed, despite the oscillatory flow [124]. Accordingly, H_2SO_4 was added to the aqueous phase in order to fully dissolve the starting material and operate under homogeneous conditions.

In a further example of solid processing using this reactor, a novel method for reduction of olefins and aromatic nitro groups was described (Fig. 14c). This method uses $NaBH_4$ as a reductant, in combination with stoichiometric $CoSO_4$. The authors state that a solid (proposed to be the catalytically active species, Co_2B) is formed, alongside H_2 gas evolution, justifying the use of an OFR. A high oscillation frequency of 3 Hz enabled gram-scale processing, where excellent yields were obtained in a short residence time of 3 min [125].

In 2020, Roberge et al. implemented a coiled baffleless OFR, combined with a bellows-based oscillatory pump, to handle solids [126]. Two reactions involving the formation of a solid were assessed. The first consisted of a reaction between cyclohexylamine (**38**) and glyoxal (**39**), forming the insoluble diimine product **40** (Fig. 15a). A batch experiment was conducted first, to characterize the reaction. When the

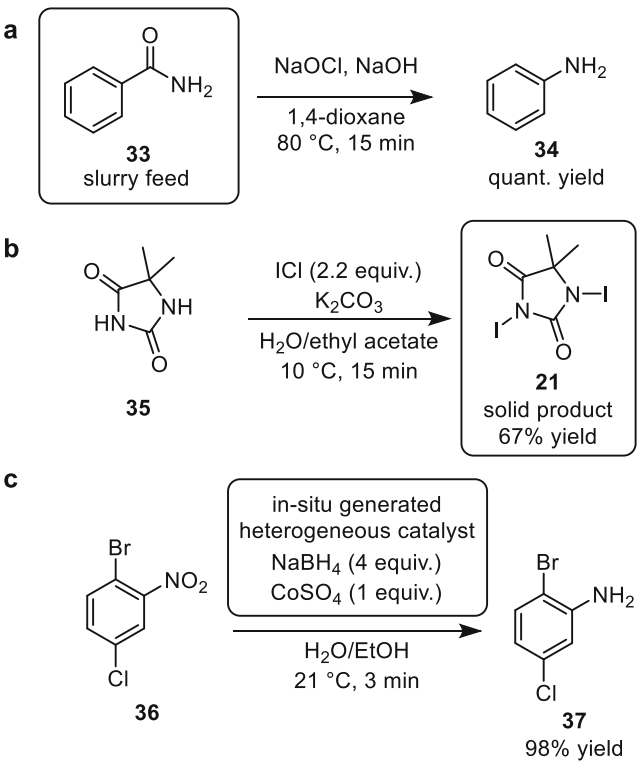

Fig. 14 Solid-liquid applications of a MJOD reactor. (**a**) Hofmann rearrangement using a slurry feed of starting material **33** (**b**) Preparation of iodinating reagent **21**, formed as a solid during the reaction (**c**) $NaBH_4$ reduction of nitro groups using an in-situ generated heterogeneous catalyst

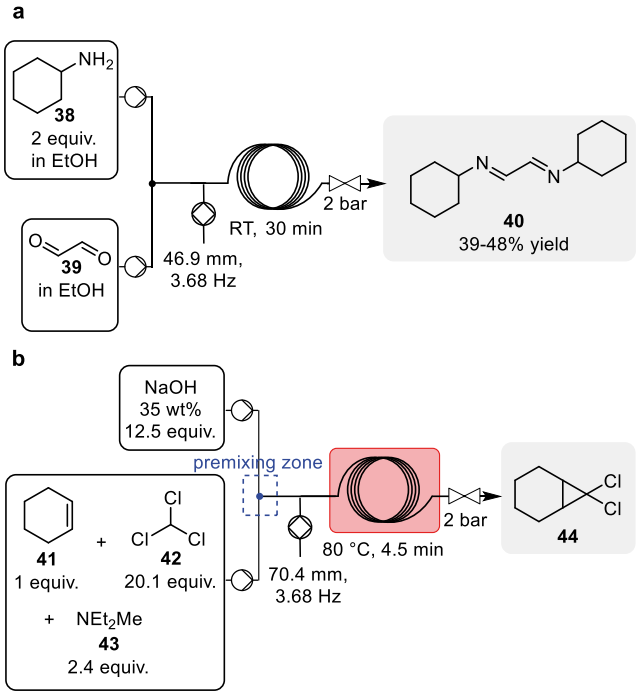

Fig. 15 Solid formation reactions in a coiled baffleless OFR (**a**) precipitation reaction for the synthesis of diimine **40** (**b**) Liquid–liquid phase transfer catalyzed reaction for the synthesis of *gem*-dichlorocyclopropane **44**, with solid by-product formation

reaction was transposed to flow, pulsations were required to avoid clogging. A yield between 39 and 48% was obtained, depending on the reagent concentrations. Using these conditions, a long run of 5 h was performed without any clogging. Lowering the oscillatory frequency and amplitude, to minimize the energy dissipation rate, had no detrimental impact on the handling of the solid.

The second reaction was a liquid-liquid reaction between dichlorocarbene, formed by the deprotonation of chloroform (**42**) with NaOH, and cyclohexene (**41**) to form 7,7-dichlorobicyclo[4.1.0]-heptane (**44**) and solid NaCl (Fig. 15b). This reaction requires a phase transfer catalyst, diethylmethylamine (**43**), to transfer the formed dichlorocarbene between the aqueous and organic phases. This reaction had already been reported under continuous flow conditions in a packed bed reactor, but had a narrow operating window due to problems with clogging [127]. Using the previously optimized conditions, clogging rapidly occurred because of a side-reaction leading to gas formation and oscillation dampening.

Characterization of the flow conditions showed that increasing the oscillation frequency led to a broadening of the RTD. However, Dean secondary flows (Table 1) were generated, which minimized solid stagnation and deposition. The particle size distribution was larger under flow than batch conditions. When the oscillation frequency was increased, smaller and less uniform particles were obtained.

Another recent application of solid handling in OFRs is at the interface between photochemistry, chemical engineering and organic chemistry. The use of heterogeneous catalysts in photochemistry has attracted attention as a replacement for expensive and toxic rare metal homogeneous catalysts, which are difficult to recycle [128–130]. Coupled with continuous flow technology, heterogeneous photochemistry becomes more reliable, safer and greener [131]. Therefore, using OFRs for heterogeneous photocatalysis is a perfect match.

A study by Kappe, Pieber et al. demonstrated the handling of solids in a baffleless OFR for C-N coupling reactions catalyzed by a carbon nitride semiconductor photocatalyst (CN-OA-m) coupled with $NiBr_2.3H_2O$ (Fig. 16a) [132]. The OFR (HANU reactor, Creaflow) consists of a series of cubic static mixing elements, providing split-and-recombine mixing (Fig. 3c). This facilitated a stable suspension in combination with an oscillatory diaphragm pulsator unit. In this case, it was essential to include a pulsation dampener and BPR to prevent suction of air or cavitation during backward pulsation.

A series of RTD measurements allowed quantification of the plug flow character, using the corresponding Bodenstein numbers for each set of oscillation parameters. The amplitude and frequency of the pulsation were optimized to ensure reaction efficiency, while maintaining a stable suspension of photocatalyst. At low frequencies and amplitudes, quantitative yields of **47** were obtained from the model reaction between 4-bromobenzoate (**45**) and pyrrolidine (**46**). It was shown that the photocatalyst could be recycled over ten cycles without significant changes in the yield. The stability, robustness and scalability of the protocol were also proven by performing a long run of 4.5 h and isolating >12 g (2.67 g h^{-1}) of aniline **47**. Finally, an intermediate (**49**) in the synthesis of the API tetracaine was synthesized with a productivity of 1.12 g h^{-1} after a slight reoptimization of the reaction conditions (Fig. 16b).

The most recent example reported for slurry handling in an OFR also considers a photochemical transformation performed in the commercial HANU reactor, reported by Debrouwer et al. [133]. Experimental and computational characterization of the oscillatory flow regime in this type of OFR were established and showed that the implementation of high oscillation amplitudes increases axial mixing. Similar trends to those determined by the Kappe group for the RTD under different oscillatory conditions were also obtained [132]. The adaptation of a heterogeneous nickel/photoredox catalyzed $C(sp^2)$-$C(sp^3)$ cross-electrophile coupling to flow was assessed. Coupling an aryl bromide (**45**) with an alkyl bromide (**50**) provided the product **51** (Fig. 17). Despite the excellent suspension properties of the OFR, sedimentation of the solid Na_2CO_3 base occured in the supply tubing to the pump. Decreasing the particle size by wet milling overcame this issue, allowing stable processing, with a high productivity of **51** (0.87 g h^{-1}).

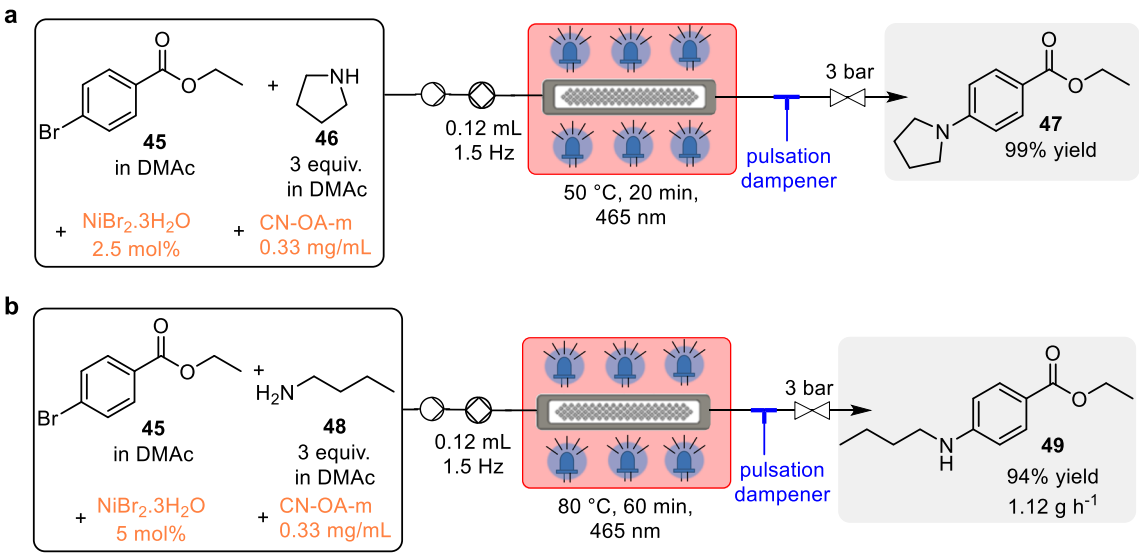

Fig. 16 C-N coupling reaction photocatalyzed by a carbon nitride semiconductor (CN-OA-m) and $NiBr_2.3H_2O$ catalyst in a microstructured OFR (**a**) optimized conditions for cross-coupling of 4-bromobenzoate **45** and pyrrolidine **46** as a model reaction (**b**) synthesis of tetracaine precursor **49**

Conclusions

Since the addition of an oscillatory flow to a net flow improves heat- and mass transfer, OFRs have already been used to overcome issues encountered by conventional flow reactors. Liquid-liquid biphasic reactions that need high mass transfer have been effectively implemented under oscillatory flow conditions. Biodiesel production in particular, which involves immiscible phases and long residence times, has been studied in-depth for over 20 years. Rational design has enhanced the assets of such reactors towards optimal baffle structures for large scale operation. The decoupling of mixing and residence time has also been recently exploited for other reactions in liquid-liquid systems, for example in small scale reaction screening.

In addition, the appealing profile of these reactors for solid-liquid reactions has first been tested in packed meso-COBRs. A deeper understanding of the effect of oscillations on the handling of solids, thanks to recent studies concerning axial dispersion, has enabled scientists to efficiently perform reactions with suspended solid particles. Nevertheless, a compromise between efficacious particle suspension and minimal axial dispersion has to be found during reaction optimization.

From this overview, it is clear that OFRs broaden the possibilities to tackle chemical challenges under continuous flow conditions. With this in mind, OFRs are certain to become a key element in the flow chemist's toolbox, particularly for slow or multiphasic reactions. The performance of OFRs can be weaker at high net flow rates or outside of the droplet flow regimes for liquid-liquid reactions. Moreover, the compressibility of gases appears to discourage their use for such applications, because of oscillation dampening. Nevertheless, the diversity of baffle geometries renders these reactors suitable for different purposes, while oscillation conditions represent novel process parameters to consider and optimize. In this way, OFRs enable a smooth transition for a wider range of chemistries from batch to flow, and can facilitate scale-up based on maintaining the system's hydrodynamic characteristics. It is anticipated that new OFR configurations will be developed in the coming years, to tackle the handling of dense solids and high solid loadings, which remain challenging for flow processing.

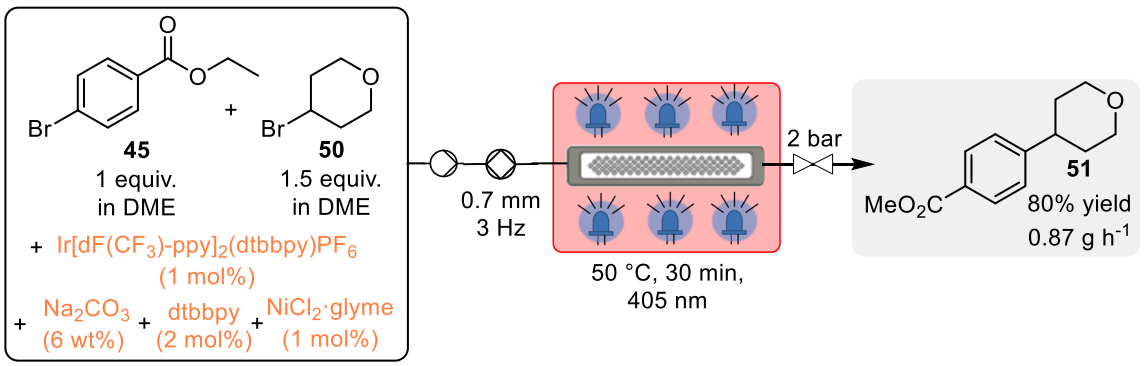

Fig. 17 Heterogeneous photocatalytic $C(sp^2)$-$C(sp^3)$ cross-electrophile coupling of aryl bromide **45** with alkyl bromide **50** in a microstructured OFR

Acknowledgements Open access funding provided by University of Graz.

Code availability Not applicable.

Funding information The CC FLOW Project (Austrian Research Promotion Agency FFG No. 862766) is funded through the Austrian COMET Program by the Austrian Federal Ministry of Transport, Innovation and Technology (BMVIT), the Austrian Federal Ministry of Science, Research and Economy (BMWFW), and by the State of Styria (Styrian Funding Agency SFG). P.B. acknowledges support by the University of Liege through the Erasmus+ funding program.

Data availability Not applicable.

Compliance with ethical standards

Conflicts of interest/competing interests Not applicable.

Open Access This article is licensed under a Creative Commons Attribution 4.0 International License, which permits use, sharing, adaptation, distribution and reproduction in any medium or format, as long as you give appropriate credit to the original author(s) and the source, provide a link to the Creative Commons licence, and indicate if changes were made. The images or other third party material in this article are included in the article's Creative Commons licence, unless indicated otherwise in a credit line to the material. If material is not included in the article's Creative Commons licence and your intended use is not permitted by statutory regulation or exceeds the permitted use, you will need to obtain permission directly from the copyright holder. To view a copy of this licence, visit http://creativecommons.org/licenses/by/4.0/.

References

1. Rehm TH (2019). ChemPhotoChem 3:1–21
2. Atobe M, Tateno H, Matsumura Y (2018). Chem Rev 118:4541–4572
3. Cambié D, Bottecchia C, Straathof NJW, Hessel V, Noël T (2016). Chem Rev 116:10276–11034
4. Gutmann B, Cantillo D, Kappe CO (2015). Angew Chem - Int Ed 54:6688–6728
5. Bezerra MA, Lemos VA, de Oliveira DM, Novaes CG, Barreto JA, Alves JPS, Cerqueira UMF da M, Santos QO dos, Araújo SA (2020). Microchem J 155:10473
6. Baumann M (2018). Org Biomol Chem 16:5946–5954
7. Britton J, Raston CL (2017). Chem Soc Rev 46:1250–1271
8. Trojanowicz M (2020). Molecules 25:1434
9. di Filippo M, Bracken C, Baumann M (2020). Molecules 25:356
10. Hommes A, Heeres HJ, Yue J (2019). ChemCatChem 11:4671–4708
11. Sui J, Yan J, Liu D, Wang K, Luo G (2019). Small 1902828:1–23
12. Berton M, de Souza JM, Abdiaj I, McQuade DT, Snead DR (2020). J Flow Chem 10:73–92
13. Stonestreet P, Harvey AP (2002). Chem Eng Res and Des 80:31–44
14. McGlone T, Briggs NEB, Clark CA, Brown CJ, Sefcik J, Florence AJ (2015). Org Process Res Dev 19:1186–1202
15. Abbott MSR, Harvey AP, Valente Perez G, Theodorou MK (2013). Interface Focus 3:20120036
16. McDonough JR, Phan AN, Harvey AP (2015). Chem Eng J 265:110–121
17. Ni X, Mackley MR, Harvey AP, Stonestreet P, Baird MHI, Rama Rao N v. (2003). Chem Eng Res Des 81:373–338
18. Ricardo C, Ni X (2009). Org Process Res Dev 13:1080–1087
19. McDonough JR, Phan AN, Harvey AP (2018). Chem Eng and Process Process Intensif 129:51–62
20. Mohd Rasdi FR, Phan AN, Harvey AP (2013). Chem Eng J 222:282–291
21. McDonough JR, Phan AN, Reay DA, Harvey AP (2016). Chem Eng Process Process Intensif 110:201–213
22. Sleveland D, Bjørsvik HR (2012). Org Process Res Dev 16:1121–1130
23. Bjørsvik HR, Liguori L (2014). Org Process Res Dev 18:1509–1515
24. Drageset A, Elumalai V, Bjørsvik HR (2018). React Chem Eng 3:550–558
25. Lucas MS, Reis NM, Li Puma G (2016). Chem Eng J 296:335–339
26. Navarro-Fuentes F, Keane M, Ni X (2019). Org Process Res Dev 23:38–44
27. Graça CAL, Lima RB, Pereira MFR, Silva AMT, Ferreira A (2020). Chem Eng J 389:124412
28. Spaccini R, Liguori L, Punta C, Bjørsvik HR (2012). ChemSusChem 5:261–265
29. McDonough JR, Murta S, Law R, Harvey AP (2019). Chem Eng J 358:643–657
30. Slavnić DS, Živković L v., Bjelić A v., Bugarski BM, Nikačević NM (2017). J Chem Technol Biotechnol 92:2178–2188
31. Smith KB, Mackley MR (2006). Chem Eng Res Des 84:1001–1011
32. Phan AN, Harvey A (2010). Chem Eng J 159:212–219
33. Zheng M, Mackley M (2008). Chem Eng Sci 63:1788–1799
34. Reis N, Vicente AA, Teixeira JA (2010). Chem Eng Process Process Intensif 49:793–803
35. Ahmed SMR, Phan AN, Harvey AP (2017). Chem Eng Technol 40:907–914
36. Mazubert A, Fletcher DF, Poux M, Aubin J (2016). Chem Eng Process Process Intensif 108:78–92
37. McDonough JR, Ahmed SMR, Phan AN, Harvey AP (2017). Chem Eng Sci 171:160–178
38. Millor GJ, Lee YC, Ni X (2019). Comp Chem Eng 124:14–27
39. Nogueira X, Taylor BJ, Gomez H, Colominas I, Mackley MR (2013). Comp Chem Eng 49:1–17
40. Phan AN, Harvey AP (2012). Chem Eng J 180:229–236
41. McDonough JR, Oates MF, Law R, Harvey AP (2019). Chem Eng J 361:508–518
42. Phan AN, Harvey A, Lavender J (2011). Chem Eng Process Process Intensif 50:254–263
43. Reis N, Harvey AP, Mackley MR, Vicente AA, Teixeira JA (2005). Chem Eng Res Des 83:357–371
44. González Niño C, Kapur N, King MF, de Boer G, Blacker AJ, Bourne R, Thompson H (2019). Int J Comput Fluid Dyn 33:317–331
45. Reintjens RWEG, Thathagar M (2011) Oscillating flow minireactor. US patent 10,118,149 B2 (Jan 13, 2011)
46. Jähnisch K, Hessel V, Löwe H, Baerns M (2004). Angew Chem - Int Ed 43:406–446
47. Mielke E, Roberge DM, Macchi A (2016). J Flow Chem 6:279–287
48. Reis N, Pereira RN, Vicente AA, Teixeira JA (2008). Ind Eng Chem Res 47:7190–7201
49. Law R, Ahmed S, Tang N, Phan A, Harvey A (2018). Chem Eng Process Process Intensif 125:133–138
50. González-Juárez D, Herrero-Martín R, Solano JP (2018). Appl Therm Eng 141:494–502
51. Solano JP, Herrero R, Espín S, Phan AN, Harvey AP (2012). Chem Eng Res Des 90:732–742

52. Ahmed SMR, Phan AN, Harvey AP (2018). Chem Eng Process Process Intensif 130:229–239
53. Jimeno G, Lee YC, Ni X (2018). Chem Eng Process Process Intensif 134:153–162
54. Avila M, Fletcher DF, Poux M, Xuereb C, Aubin J (2020). Chem Eng Sci 212:115310
55. Ni X, Zhang Y, Mustafa I (1998). Chem Eng Sci 53:2903–2919
56. Ni X, Zhang Y, Mustafa I (1999). Chem Eng Sci 54:841–850
57. Ni X, Johnstone JC, Symes KC, Grey BD, Bennett DC (2001). AIChE 47:1746–1757
58. Ni X, Murray KR, Zhang Y, Bennett D, Howes T (2002). Powder Technol 124:281–286
59. Harvey AP, Mackley MR, Stonestreet P (2001). Ind Eng Chem Res 40:5371–5377
60. Mohd GATI, Resul MFMG, Yunus R, Yaw TCS (2008). Sci Technol 3:138–145
61. Zheng M, Skelton RL, Mackley MR (2007). Process Saf Environ Prot 85:365–371
62. Harvey AP, Mackley MR, Seliger T (2003). J Chem Technol Biotechnol 78:338–341
63. Phan AN, Harvey AP, Rawcliffe M (2011). Fuel Process Technol 92:1560–1567
64. Sagmeister P, Poms J, Williams JD, Kappe CO (2020). React Chem Eng 5:677–684
65. Hone CA, Holmes N, Akien GR, Bourne RA, Muller FL (2017). React Chem Eng 2:103–108
66. Moore JS, Jensen KF (2014). Angew Chemie - Int Ed 53:470–473
67. Phan AN, Harvey AP, Eze V (2012). Chem Eng Technol 35: 1214–1220
68. Al-Saadi LS, Alegría A, Eze VC, Harvey AP (2019). Chem Eng Technol 42:539–548
69. Al-Saadi LS, Eze VC, Harvey AP (2020). Biofuels. https://doi.org/10.1080/17597269.2020.1727688
70. Mazubert A, Aubin J, Elgue S, Poux M (2014). Green Process Synth 3:419–429
71. Mazubert A, Crockatt M, Poux M, Aubin J, Roelands M (2015). Chem Eng Technol 38:2161–2169
72. Lobry E, Lasuye T, Gourdon C, Xuereb C (2015). Chem Eng J 259:505–518
73. Abolhasani M, Bruno NC, Jensen KF (2015). Chem Commun 51: 8916–8919
74. Abolhasani M, Oskooei A, Kumacheva E, Günther A (2014). Lab Chip 14:2309–2318
75. Gielen F, Van Vliet L, Koprowski BT, Devenish SRA, Fischlechner M, Edel JB, Niu X, deMello AJ, Hollfelder, F (2013). Anal Chem 85:4761–4769
76. Abolhasani M, Coley CW, Xie L, Chen O, Bawendi MG, Jensen KF (2015). Chem Mater 27:6131–6138
77. Shen Y, Abolhasani M, Chen Y, Xie L, Yang L, Coley CW, Bawendi MG, Jensen KF (2017). Angew Chem - Int Ed 56: 16333–16337
78. Coley CW, Abolhasani M, Lin H, Jensen KF (2017). Angew Chem - Int Ed 56:9847-9850
79. Hwang YJ, Coley CW, Abolhasani M, Marzinzik AL, Koch G, Spanka C, Lehmann H, Jensen KF (2017). Chem Commun 53: 6649–6652
80. Hsieh HW, Coley CW, Baumgartner LM, Jensen KF, Robinson RI (2018). Org Process Res Dev 22:542–550
81. Mongeon SS, Roberge DM, Bittel M, Elsner P, Macchi A (2016). Org Process Res Dev 20:733–741
82. Rafiee SE, Sadeghiazad MM (2017). Appl Therm Eng 114:300–327
83. Loponov KN, Deadman BJ, Zhu J, Rielly C, Holdich RG, Hii KK, Hellgardt K (2017). Chem Eng J 329:220–230
84. Liguori L, Bjørsvik HR (2007) Continuous flow reactor. World patent WO 2007/058544 A1, Nov 17, 2006
85. Liguori L, Bjørsvik HR (2011). Org Process Res Dev 15:997–1009
86. Drageset A, Frøystein NÅ, Törnroos KW, Bjørsvik HR (2019). React Chem Eng 4:41–51
87. Schoenitz M, Grundemann L, Augustin W, Scholl S (2015). Chem Commun 51:8213–8228
88. Kashani S, Sullivan RJ, Andersen M, Newman SG (2018). Green Chem 20:1748–1753
89. Heider PL, Born SC, Basak S, Benyahia B, Lakerveld R, Zhang H, Hogan R, Buchbinder L, Wolfe A, Mascia S, Evans JMB, Jamison TF, Jensen KF (2014). Org Process Res Dev 18:402–409
90. Hartman RL (2012). Org Process Res Dev 16:870–887
91. Wang Z, Gérardy R, Gauron G, Damblon C, Monbaliu JCM (2019). React Chem Eng 4:17–26
92. Colella M, Carlucci C, Luisi R (2018). Top Curr Chem 376:46
93. Munirathinam R, Huskens J, Verboom W (2015). Adv Synth Catal 357:1093–1123
94. Rodríguez-Escrich C, Pericàs MA (2018). Chem Rec 18:1–20
95. Pomberger A, Mo Y, Nandiwale KY, Schultz VL, Duvadie R, Robinson RI, Altinoglu EI, Jensen KF (2019). Org Process Res Dev 23:2699–2706
96. Mo Y, Jensen KF (2016). React Chem Eng 1:501–507
97. Chapman MR, Kwan MHT, King G, Jolley KE, Hussain M, Hussain S, Salama IE, González Nino C, Thompson LA, Bayana ME, Clayton AD, Nguyen BN, Turner NJ, Kapur N, Blacker AJ (2017). Org Process Res Dev 21:1294–1301
98. Filipponi P, Gioiello A, Baxendale IR (2016). Org Process Res Dev 20:371–375
99. Browne DL, Deadman BJ, Ashe R, Baxendale IR, Ley SV (2011). Org Process Res Dev 15:693–697
100. Falß S, Tomaiuolo G, Perazzo A, Hodgson P, Yaseneva P, Zakrzewski J, Guido S, Lapkin A, Woodward R, Meadows RE (2016). Org Process Res Dev 20:558–567
101. Noël T, Naber JR, Hartman RL, McMullen JP, Jensen KF, Buchwald SL (2011). Chem Sci 2:287–290
102. Cao Q, Howard JL, Crawford DE, James SL, Browne DL (2018). Green Chem 20:4443–4447
103. Isoni V, Mendoza K, Lim E, Teoh SK (2017). Org Process Res Dev 21:992–1002
104. Sharma BM, Atapalkar RS, Kulkarni AA (2019). Green Chem 21: 5639–5646
105. Crawford DE, Miskimmin CK, Cahir J, James SL (2017). Chem Commun 53:13067–13070
106. Bannock JH, Krishnadasan SH, Nightingale AM, Yau CP, Khaw K, Burkitt D, Halls JJM, Heeney M, de Mello JC (2013). Adv Funct Mater 23:2123–2129
107. Poe SL, Cummings MA, Haaf MP, McQuade DT (2006). Angew Chem - Int Ed 45:1544–1548
108. Slavnić D, Bugarski B, Nikačević N (2019). Chem Eng Process Process Intensif 135:108–119
109. Ejim LN, Yerdelen S, McGlone T, Onyemelukwe I, Johnston B, Florence AJ, Reis NM (2017). Chem Eng J 308:669–682
110. Kacker R, Regensburg SI, Kramer HJM (2017). Chem Eng J 317: 413–423
111. Cruz P, Silva C, Rocha F, Ferreira A (2019). AIChE 65:e16683
112. Oliva JA, Pal K, Barton A, Firth P, Nagy ZK (2018). Chem Eng J 351:498–505
113. Onyemelukwe II, Nagy ZK, Rielly CD (2020). Chem Eng J 382: 122862
114. Fabiyi ME, Skelton RL (1999) J Photochem Photobiol. A 129:17–24
115. Fabiyi ME, Skelton RL (2000). Trans IChemE 78:399–404
116. Gao P, Han Ching W, Herrmann M, Kwong Chan C, Yue PL (2003). Chem Eng Sci 58:1013–1020
117. Eze VC, Phan AN, Pirez C, Harvey AP, Lee AF, Wilson K (2013). Catal Sci Tech 3:2373–2237

118. Eze VC, Fisher JC, Phan AN, Harvey AP (2017). Chem Eng J 322:205–214
119. Eze VC, Harvey AP (2018). Chem Eng J 347:41–51
120. Kefas HM, Yunus R, Rashid U, Taufiq-Yap YH (2019). J Environ Chem Eng 7:102993
121. Okafor O, Weilhard A, Fernandes JA, Karjalainen E, Goodridge R, Sans V (2017). React Chem Eng 2:129–136
122. Zheng H, Yan Z, Chu S, Chen J (2018). Chem Eng Process Process Intensif 134:1–8
123. Ferreri M, Drageset A, Gambarotti C, Bjørsvik HR (2016). React Chem Eng 1:379–386
124. Drageset A, Bjørsvik HR (2016). React Chem Eng 1:436–444
125. Lundevall FJ, Elumalai V, Drageset A, Totland C, Bjørsvik HR (2018). Eur J Org Chem 2018:3416–3425
126. Doyle BJ, Gutmann B, Bittel M, Hubler T, MacChi A, Roberge DM (2020). Ind Eng Chem Res 59:4007–4019
127. von Keutz T, Cantillo D, Kappe CO (2019). J Flow Chem 9:27–34
128. Gisbertz S, Pieber B (2020). ChemPhotoChem 4:1–21
129. Riente P, Noël T (2019). Catal Sci Technol 9:5186–5232
130. Savateev A, Ghosh I, König B, Antonietti M (2018). Angew Chem - Int Ed 57:15936–15947
131. Williams JD, Kappe CO (2020). Curr Opin Green Sustain Chem 25:100351
132. Rosso C, Gisbertz S, Williams JD, Gemoets H, Debrouwer W, Pieber B, Kappe CO (2020). React Chem Eng 5:595–604
133. Debrouwer W, Kimpe W, Dangreau R, Huvaere K, Gemoets HPL, Mottaghi M, Kuhn S, Van Aken K (2020). Org Process Res Dev. https://doi.org/10.1021/acs.oprd.0c00150

Publisher's note Springer Nature remains neutral with regard to jurisdictional claims in published maps and institutional affiliations.